binding and presumably sequestering TCF1 and/or modifying its activity.

To determine whether SOX13 is necessary for γδ T cell development, we generated Sox13-deficient mice. Because of as-yet-uncharacterized developmental abnormalities in postnatal Sox13$^{-/-}$ mice (fig. S6), we determined the effect of Sox13-deficiency during embryonic development where there are no overt developmental defects. No significant differences were observed in the proportions of αβ-lineage thymocytes at E18.5 (Fig. 4A). However, there was a gene dose–dependent decrease in the number and proportion of γδTCR$^+$ cells in Sox13$^{+/-}$ and Sox13$^{-/-}$ mice as compared to LMCs (Fig. 4, A and B), resulting in a significantly increased ratio of the absolute number of mature αβ-lineage thymocytes relative to γδTCR$^+$ thymocytes (Fig. 4C). This adverse effect of Sox13 deficiency on γδ T cell development was evident despite the fact that Sox13$^{-/-}$ mice expressed Sox5, the closest relative of Sox13 (24), whose expression pattern is identical to that of Sox13 during mouse T cell development (fig. S6). In addition, Sox13$^{-/-}$ γδ and TN thymocytes exhibited significantly enhanced rates of proliferation (Fig. 4D), a corollary finding to reduced proliferation of TN thymocytes in Sox13Tg mice (Fig. 2E). These results indicate that the developing γδ thymocytes are extremely sensitive to the levels of SOX13 and that SOX13 is necessary for normal γδ T cell development.

Sox13 is the first true γδ-lineage–specific TF identified that is necessary for normal γδ T cell development. The heterogeneous expression of Sox13 in TN2 cells, combined with the asymmetry in the developmental potential of the TN2 subset, indicates that some lineage separation had occurred before TCR rearrangement. The silencing of Sox13 expression may constitute an initial step in the elaboration of the αβ-lineage molecular program. Although this conclusion does not preclude the influence of possibly distinct γδTCR and preTCR signaling modules in subsequently reinforcing or modifying the lineage-fate decision, the ability of SOX13 to antagonize TCF1 suggests that a simple on/off switch controlling the magnitude of Wnt/TCF1 signaling may be an early, critical regulator of the binary T cell–fate decision process.

References and Notes
1. A. C. Hayday, *Annu. Rev. Immunol.* **18**, 975 (2000).
2. S. H. Kaufmann, *Proc. Natl. Acad. Sci. U.S.A.* **93**, 2272 (1996).
3. C. Saint-Ruf et al., *Nature* **406**, 524 (2000).
4. J. P. Allison, L. L. Lanier, *Immunol. Today* **8**, 293 (1987).
5. I. Ishida et al., *Proc. Natl. Acad. Sci. U.S.A.* **87**, 3067 (1990).
6. J. Kang, D. H. Raulet, *Semin. Immunol.* **9**, 171 (1997).
7. J. Roose et al., *Nucleic Acids Res.* **26**, 469 (1998).
8. Materials and methods are available as supporting material on *Science* Online.
9. B. Silva-Santos, D. J. Pennington, A. C. Hayday, *Science* **307**, 925 (2005).
10. J. Kang, A. Volkmann, D. H. Raulet, *J. Exp. Med.* **193**, 689 (2001).
11. M. Ciofani, G. C. Knowles, D. L. Wiest, H. von Boehmer, J. C. Zuniga-Pflucker, *Immunity* **25**, 105 (2006).
12. V. Ioannidis, F. Beermann, H. Clevers, W. Held, *Nat. Immunol.* **2**, 691 (2001).
13. O. Tetsu, F. McCormick, *Nature* **398**, 422 (1999).
14. E. M. Sampson et al., *EMBO J.* **20**, 4500 (2001).
15. S. Verbeek et al., *Nature* **374**, 70 (1995).
16. M. W. Schilham et al., *J. Immunol.* **161**, 3984 (1998).
17. Z. Huang et al., *J. Immunol.* **176**, 4880 (2006).
18. M. van de Wetering et al., *Cell* **88**, 789 (1997).
19. F. J. Staal et al., *Eur. J. Immunol.* **31**, 285 (2001).
20. L. Kan et al., *Dev. Biol.* **269**, 580 (2004).
21. A. M. Zorn et al., *Mol. Cell* **4**, 487 (1999).
22. V. Korinek et al., *Science* **275**, 1784 (1997).
23. W. Held, B. Kunz, B. Lowin-Kropf, M. van de Wetering, H. Clevers, *Immunity* **11**, 433 (1999).
24. M. Wegner, *Nucleic Acids Res.* **27**, 1409 (1999).
25. We thank D. Raulet, L. Berg, and M. Bix for helpful comments; L. Scarpellino for technical assistance; and the transgenic, FACS, and genomics services at the University of Massachusets. Supported by the Swiss National Science Foundation and the Leenaards Foundation (W.H.) and National Cancer Institute grant RO1CA100382/92614 (J.K.).

A Systems Approach to Measuring the Binding Energy Landscapes of Transcription Factors

Sebastian J. Maerkl[1,2] and Stephen R. Quake[2]*

A major goal of systems biology is to predict the function of biological networks. Although network topologies have been successfully determined in many cases, the quantitative parameters governing these networks generally have not. Measuring affinities of molecular interactions in high-throughput format remains problematic, especially for transient and low-affinity interactions. We describe a high-throughput microfluidic platform that measures such properties on the basis of mechanical trapping of molecular interactions. With this platform we characterized DNA binding energy landscapes for four eukaryotic transcription factors; these landscapes were used to test basic assumptions about transcription factor binding and to predict their in vivo function.

Systems biology focuses on understanding the collective properties of biological networks; these networks in turn describe interactions between as many as thousands of unique elements. In recent years, knowledge of biological networks has grown dramatically, mainly because of the development and application of novel genomic (1–3) and proteomic methods (4–8) as well as bottom-up approaches such as genetic network engineering (9, 10). But as networks topologies are becoming well characterized, information about the elements comprising these networks has remained minimal and in the realm of low-throughput biology. In order to model and predict the behavior of these complex systems, the underlying interactions between elements will have to be quantitatively characterized.

Quantifying the affinities of molecular interactions is a considerable technical challenge.

First, any particular biological interaction is governed by a large number of variables. Therefore, obtaining equilibrium dissociation constants requires one to perform dozens of assays as the concentrations of various components are systematically varied, increasing the number of measurements needed in an already logistically challenging problem. A second and more fundamental problem is the fact that many molecular interactions are transient and exhibit nanomolar to micromolar affinities, leading to rapid loss of bound material or little bound material in the first place. These factors are problematic for high-throughput methods such as yeast two-hybrid (6) and tandem affinity purification mass spectrometry (4, 5), where transient interactions are frequently missed. Protein-protein (11) and protein-DNA binding microarrays (PBMs) (12–14) are especially susceptible because of their stringent wash requirements, causing rapid loss of weakly bound material. Protein arrays have been applied to quantify ligand–ErbB receptor inter-

[1]Biochemistry and Molecular Biophysics Option, California Institute of Technology, 1200 East California Boulevard, Pasadena, CA 91125, USA. [2]Department of Bioengineering, Stanford University and Howard Hughes Medical Institute, 318 Campus Drive, Stanford, CA 94305, USA.

*To whom correspondence should be addressed. E-mail: quake@stanford.edu

actions (*11*), with off rates determined by surface plasmon resonance to be on the order of 10^{-4} s^{-1} (*15*). PBMs have been applied in a semiquantitative manner to transcription factor (TF) motif analysis for high-affinity interactions, with off rates on the order of 10^{-3} s^{-1} (*12–14*).

We developed a high-throughput microfluidic platform (Fig. 1) capable of detecting low-affinity transient binding events on the basis of the mechanically induced trapping of molecular interactions (MITOMI), which eliminates the off-rate problem facing current array platforms and allows for absolute affinity measurements. We used MITOMI to map the binding energy landscapes of four eukaryotic TFs belonging to the basic helix-loop-helix (bHLH) family by collecting over 41,000 individual data points from more than 17 devices and covering titrations over 464 target DNA sequences. These binding energy topographies allowed us to (i) predict in vivo function for two yeast TFs, (ii) make a comprehensive test of the base additivity assumption, and (iii) test the hypothesis that the basic region alone determines binding specificity of bHLH TFs.

bHLH motifs represent the third largest TF family in eukaryotes and regulate a wide variety of cellular functions ranging from cell proliferation and development to metabolism (*16*). We studied isoforms A and B of the human TF MAX, which together with other bHLH members play a role in cellular proliferation and many cancers (*17*). We also studied the yeast TFs Pho4p and Cbf1p; the former regulates phosphate metabolism (*18*, *19*), whereas the latter regulates methionine synthesis as well as chromosome segregation, serving a structural role in the kinetochore (*20–22*). bHLH TFs generally bind to a consensus sequence of 5′-CANNTG-3′ (where N is any nucleotide) called enhancer box (E-box) (fig. S1, A and B), which was later found to be the second most conserved motif in higher eukaryotes (*3*). Members of the bHLH family show mid- to low nanomolar DNA binding affinities and have off rates above 10^{-2} s^{-1} for their consensus sequences (*23*, *24*), with orders of magnitude higher off rates for nonconsensus sequences. This transience makes the use of conventional microarrays impractical.

The TF binding energy topographies were measured with highly integrated microfluidic devices (*25*, *26*) containing 2400 independent unit cell experiments (Fig. 1, A and B). Each device is controlled by 7233 valves fabricated by multilayer soft lithography (MSL) (*27*) and programmed with a 2400-spot DNA microarray (*28*). The 2400 chambers are arranged into 24 rows addressed via a resistance equalizer (Fig. 1A); this ensures that flow velocities are equal across all rows, resulting in uniform surface derivatization and TF deposition. To avoid time-consuming cloning and protein synthesis and purification steps, we synthesized the

TFs in situ via wheat germ–based in vitro transcription and translation (ITT). We designed a two-step polymerase chain reaction (PCR) method that generates linear expression–ready templates directly from yeast genomic DNA or cDNA clones (fig. S2). This approach allowed us to not only rapidly screen new TFs but also easily create and test structural chimeras.

We synthesized libraries of Cy5-labeled target DNA sequences that comprehensively cover the E-box motif and flanking bases by permuting up to four bases at a time (fig. S1C and data set 1). Dilution series for each target DNA sequence were spotted as microarrays with column and row pitches of 563 μm and 281 μm, respectively. These arrays were used to program the microfluidic devices by aligning
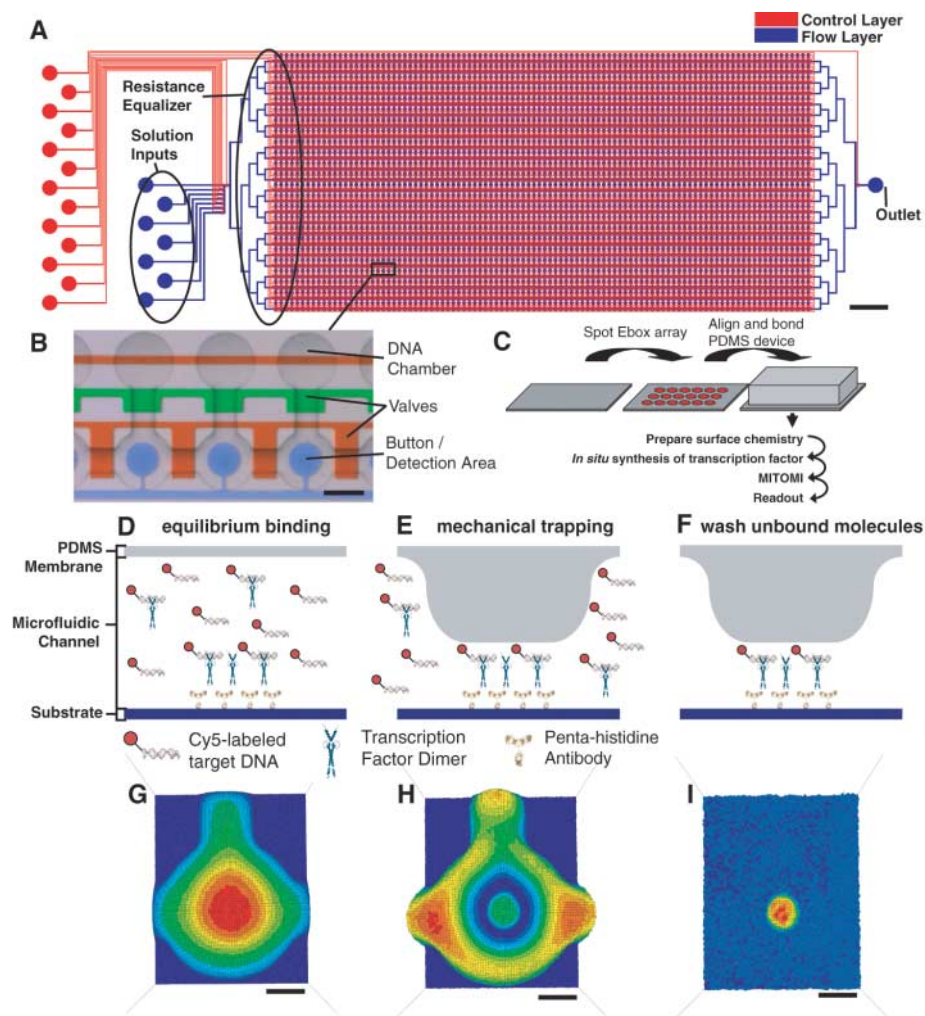

Fig. 1. (**A**) Design drawing of the microfluidic device. Red and blue lines represent control and flow channels, respectively. The device contains 2400 unit cells controlled by 7233 valves (scale bar indicates 2 mm). (**B**) Optical micrograph of three unit cells. Control channels are filled with colored food dyes for visualization. Each unit cell consists of a DNA chamber aligned to a microarray spot and a detection area. The valves shown in green control access to the DNA chambers, whereas the orange valves compartmentalize the unit cells. The button membrane is shown in blue and represents the area where detection takes place (scale bar, 150 μm). (**C**) Schematic outline of the approach. First, a microarray of target DNA sequences is spotted onto an epoxy slide. The microarray is then aligned and bonded to a microfluidic device. Next, the necessary surface chemistry is prepared, followed by in situ synthesis of TF and detection of interactions by MITOMI. (**D** to **F**) Schematic of the process of MITOMI. The gray structure at the top of each panel represents the deflectable button membrane that may be brought into contact with the glass surface (blue). (D) His$_5$-tagged TFs are localized to the surface, and TF-DNA binding is in a steady state. (E) The button membrane is brought into contact with the surface, expelling any solution phase molecules while trapping surface-bound material. (F) Unbound material not physically protected is washed away, and the remaining molecules are quantified. (**G** to **I**) Fluorescent intensity maps of target DNA concentration. (G) to (I) correspond to the states schematically shown in (D) to (F) (scale bars, 50 μm).

each spot to a unit cell. The ability to program devices with microarrays simplifies the microfluidic infrastructure and increases unit cell density. The use of microarrays for device programming is highly modular because any soluble substance or suspension may be arrayed, and it provides an elegant and efficient solution to the world-to-chip interface problem. Approximately attomoles of DNA and TF are required for each data point.

Each unit cell is controlled by three micromechanical valves (27) as well as a "button" membrane (fig. S3) used for surface derivatization and MITOMI (Fig. 1, B to I,

and fig. S4). When the button is actuated, it physically blocks a 60-μm circular area on the slide, preventing molecules from entering or leaving that part of the surface. The contact area can be precisely modulated by choice of button diameter and closing pressures (fig. S3). During surface derivatization, a circular area is masked with the button, while the rest of the surface is passivated with biotinylated bovine serum albumin. When the button is released, the previously protected circular area is specifically functionalized with biotinylated antibody against His$_5$ (fig. S4, C to G). After surface pat-

terning, the device is loaded with wheat germ–based ITT mixture containing linear DNA template coding for the TF to be synthesized, and each unit cell is isolated by closing a set of micromechanical valves. The device is incubated at 30°C for 90 min to complete TF synthesis, solvation of target DNA, and equilibration of TF and target DNA (fig. S4, H and I). After the incubation period, MITOMI is performed by again actuating the button membrane and trapping surface-bound complexes (Fig. 1, D to I, and fig. S4, J to L). Initial contact of the membrane with the surface occurs medially and extends radially outward. Radial closure prevents solvent pockets from forming between the two interfaces and effectively creates zero dead volume while preserving the equilibrium concentrations of the molecular interactions to be detected. The trapped molecules are subsequently quantified with a DNA array scanner (fig. S5). Device characterization and control experiments are described in the Supporting Online Material (figs. S6 to S8) (26); we determined the lower limit of detection to be $K_d \approx 18$ μM and established a global measurement error of 19% (fig. S9).

Our measurements agree with previous reports that the optimal binding sequence for all four TFs is CACGTG for N_{-3} to N_3 (Fig. 2, A to D, and figs. S10, A to D, and S11). We measured consensus binding affinities of 67.0 nM, 73.1 nM, 11.1 nM, and 16.6 nM for MAX isoform A, MAX isoform B, Pho4p, and Cbf1p, respectively. The binding affinity of MAX to a slightly different sequence has been measured independently and is in agreement with our result for that sequence (24). Each binding energy landscape exhibits topographic fine structures, such as affinity spikes for sequences with a one-base spacer between the two half sites (CACGGTG for example) as well as consensus neighbors CATGTG, CTCGTG, and CAGGTG. These fine structures often lie in the low-affinity regime (with off rates on the order of 2 to 20 s^{-1}) and have thus far not been observed with other methods. The binding energy landscapes for both MAX isoforms are more rugged than the landscapes of Pho4p and Cbf1p, showing strong affinities for consensus neighbors, whereas Pho4p and Cbf1p are singularly specific for the E-box consensus. These differences in topography are intriguing, because crystal structures of truncated versions of MAX and Pho4p show that both TFs make essentially the same base-specific contacts (29, 30). Therefore, similar base-specific contacts give rise to recognition of the same consensus sequence but not necessarily to similar overall binding topographies.

Informatic methods for TF binding motif discovery often rely on ad hoc hypotheses such as the additivity assumption, which
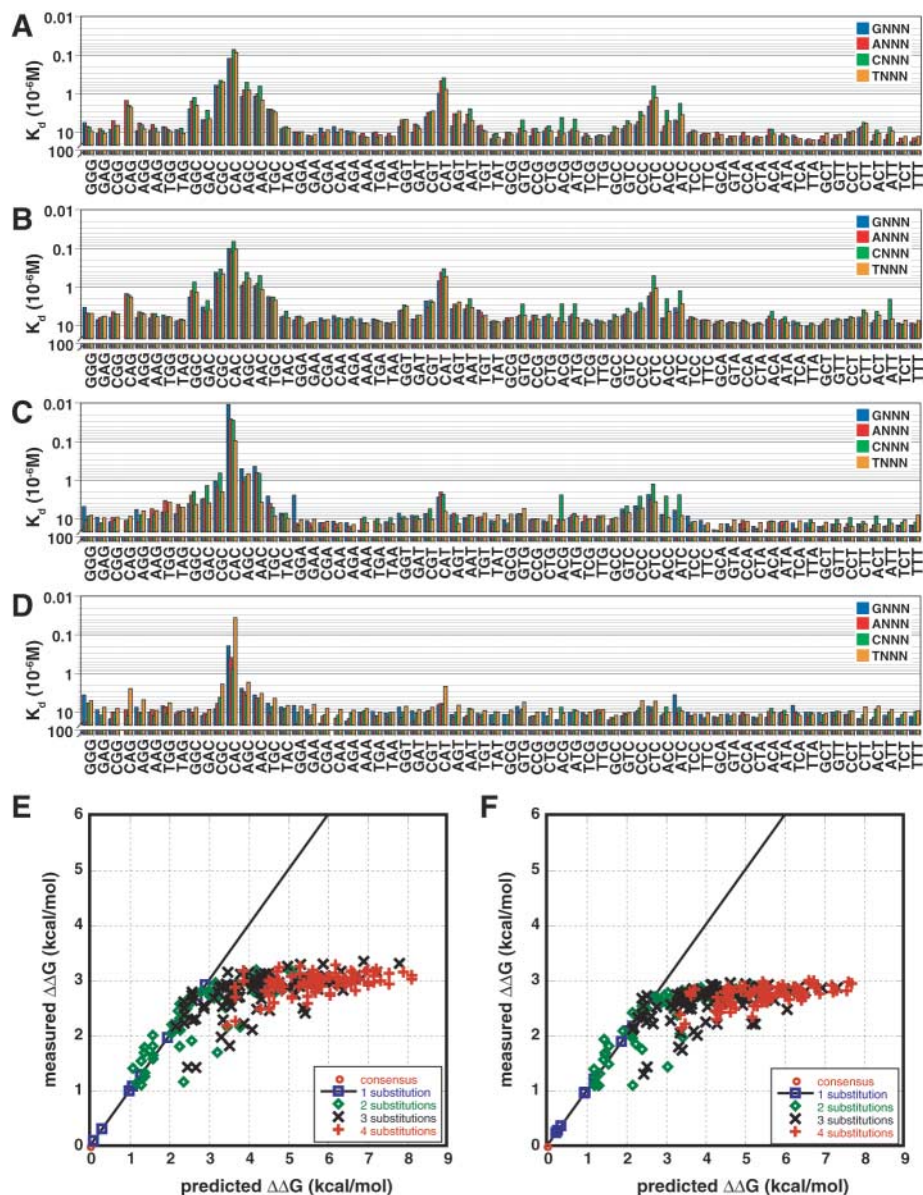

Fig. 2. Binding affinities of C-terminally tagged TFs MAX iso A (**A**), MAX iso B (**B**), Pho4p (**C**), and Cbf1p (**D**) to all sequence permutations of N_{-4} to N_{-1}. Sequences N_{-3} to N_{-1} are plotted on the category axis, with the fourth base, N_{-4}, displayed as clusters of four columns per category. (**E** and **F**) Comparisons of predicted changes in the Gibbs free energy ($\Delta\Delta G$) against measured values for MAX isoforms A and B are shown, respectively. All predicted values were calculated from PWMs assuming base independence.

posits that the energetic or informatic role of each base in a given motif is independent of the identity of neighboring bases. Evidence from small data sets contradicts this assumption (31, 32), but there is an ongoing debate on the importance of the observed non-independence (33). Our data on the absolute binding affinities of the MAX isoforms to all possible sequence permutations of one E-box half site plus a flanking base, or 256 sequences in total, allowed us to determine the extent of interdependence between individual base contacts. First, we generated a position weight matrix (PWM) for each isoform, consisting of changes in the Gibbs free energy for all 16 possible single-base substitutions. These PWMs were then used to calculate binding affinities to all 256 sequences. Because PWMs contain no information on higher-order interactions, the predicted affinities reflect an assumption of completely independent base contacts. Comparing our experimentally determined values with the predictions showed that only a small subset of values agreed (Fig. 2, E and F, and fig. S10, E and F). PWMs fail to predict low-affinity binding, because almost no sequences above 2.5 kcal/mol agreed with measured values (defined as lying within 2σ or ± 0.4

kcal/mol of the measured value). This is mostly due to the increasing role of non-specific interactions, for which failure of the PWM is not surprising. More importantly, PWMs also fail for higher affinities, predicting only 44% of all sequences below 2.5 kcal/mol. The PWMs predicted only 56%, 10%, and 0% of all double, triple, and quadruple substitutions, respectively. The consequences of these results are twofold. First, for gene discovery applications PWMs will give low false positives but more potential false negatives or missed genes. Second, PWMs are not sufficient for more detailed computational approaches to systems biology that seek to understand the stochastic dynamics of TF binding.

To address the question of how Pho4p and Cbf1p serve distinct biological functions while recognizing seemingly identical consensus motifs, we measured the extent to which these TFs recognize bases flanking the E-box consensus. Current experimental and bioinformatic methods (1, 7, 34, 35) failed to show definite differences in sequence recognition between these two TFs (CACGTGsG and rTCACGTG for Pho4p and Cbf1p, respectively, where r is any purine and s is G or C). We measured all possible permutations of three flanking bases 5′

as well as 3′ of the consensus sequence in order to determine how far base-specific recognition extends. The results show that Pho4p specifically recognizes two flanking bases, extending the consensus motif to a palindromic decamer of 5′-CCCACGTGGG-3′ (Fig. 3A and fig. S12, A and B). For Cbf1p, the flanking base recognition profile differed drastically from Pho4p, preferring GT as $N_{-5}N_{-4}$ (Fig. 3B) and the palindrome AC for N_4N_5 (fig. S12, C to D). Furthermore T and C were preferred for N_6 (A and G in terms of N_{-6}), extending Cbf1p sequence recognition from the initial hexamerous E-box motif to a dodecamer of 5′-[A/G]GTCACGTGAC[T/C]-3′.

On the basis of structural (29, 30) and biochemical data, it is widely assumed that the sequence-specific binding of bHLH TFs is determined entirely by the basic region. We assessed whether the basic region itself is sufficient to produce the observed flanking base sequence specificity by cloning the basic regions of Pho4p and Cbf1p into the MAX isoform B backbone. The results show that, despite the existence of a few intriguing sequence outliers, the basic region itself is sufficient to transform the original MAX isoform B recognition pattern to patterns resembling Pho4p and Cbf1p (Fig. 3D).

Last, we asked whether the binding energy landscapes for Pho4p and Cbf1p are sufficient to predict which genes these TFs physically bind and therefore likely regulate. We applied a simple in silico model based on calculating a probability of occupancy (P_{occ}) (36, 37) for each regulatory sequence of 5814 yeast genes and obtained 38 and 24 genes bound by Pho4p and Cbf1p, respectively. (Fig. 4, A and B, and data sets 2 and 3). We then tested whether these gene sets were significantly enriched for functions related to Pho4p (phosphate metabolism) and Cbf1p (methionine metabolism and chromosome segregation). The Pho4p data set showed significant enrichment in genes functioning in ionic homeostasis and phosphate metabolism (table S1), with 60% of the genes in the data set functioning in phosphate metabolism (37%), ionic homeostasis (13%), and vacuoles (10%) (Fig. 4A). Chromatin immunoprecipitation (ChIP)–chip and microarray experiments determining Pho4p-regulated genes have only 18% agreement; our data set includes all of these overlapping genes and has 40% agreement with at least one of the other data sets (Fig. 4E). For Cbf1p, the functional enrichment returned categories mainly involved in cell cycle and cell growth (table S1), implying that Cbf1p functions in chromosome segregation. Of Cbf1p-regulated genes, 30% are involved in chromosome structure, and another 25% are involved in budding (Fig. 4B). Only two genes (8%) regulate methionine synthesis. We also found three genes (STE20, GAL2, and DRS2) that
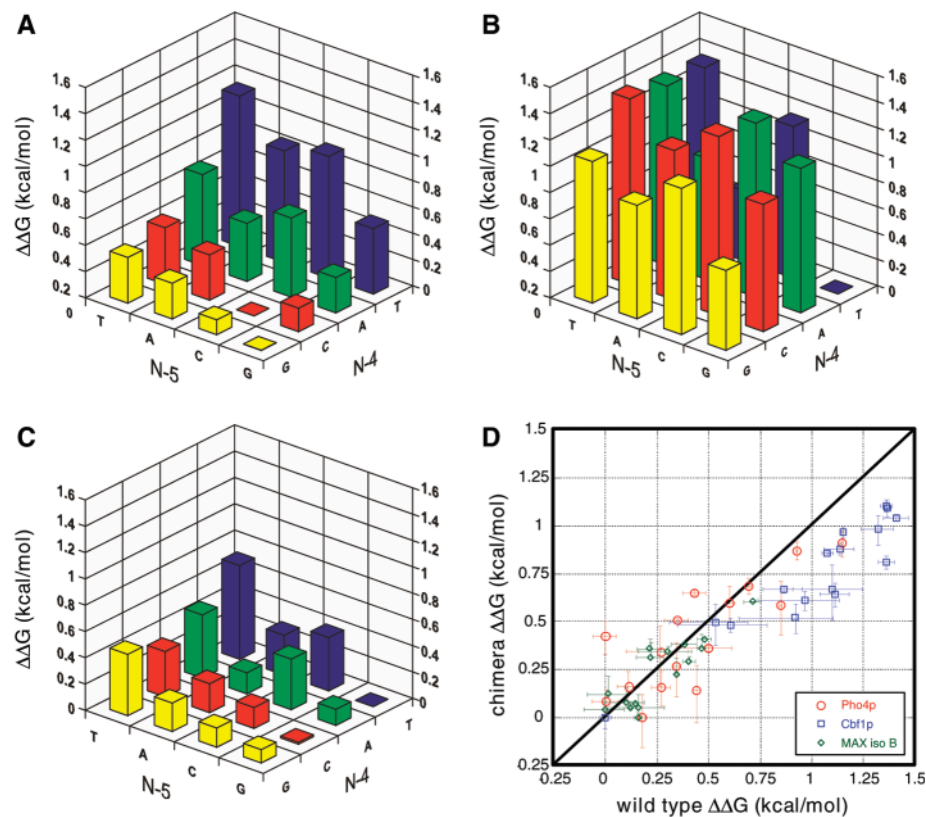

Fig. 3. $\Delta\Delta G$ values of all permutations of the two flanking bases $N_{-5}N_{-4}$ for Pho4p (**A**), Cbf1p (**B**), and MAX iso B (**C**). (**D**) Comparison of the $\Delta\Delta G$ values of the wild-type proteins shown in (A) to (C) with basic region chimeras in which the basic region of MAX isoform B was replaced by the basic regions of Pho4p, Cbf1p, and MAX iso B. The average of two experimental values is plotted, with the difference shown by the error bars.
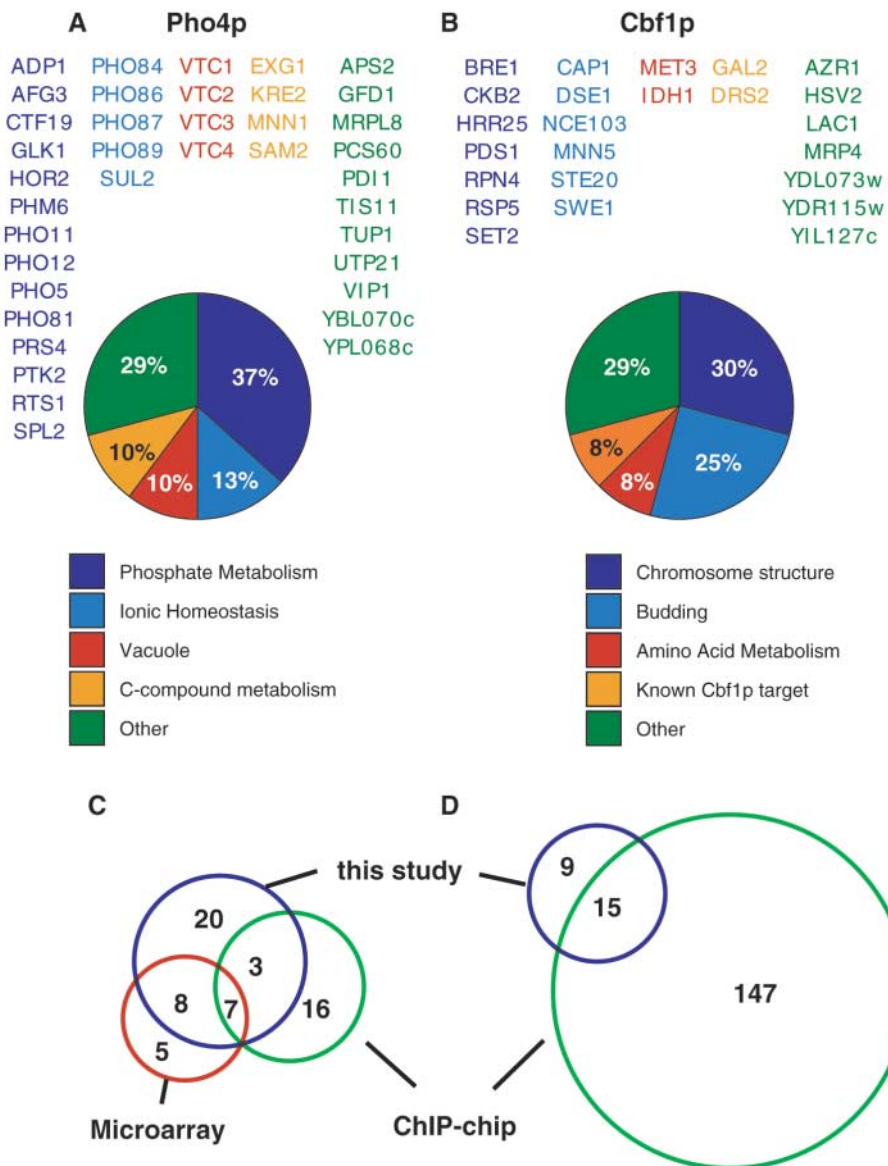
Fig. 4. In vivo function prediction for Pho4p and Cbf1p. (**A** and **B**) Genes with regulatory sequences determined to be bound by our in silico method. All genes shown here have a P_{occ} of above 0.2 and a sensu stricto conservation score of 25% or above. Pie charts show the functional distribution of the gene sets. (**C** and **D**) Venn diagrams comparing our predicted gene sets to gene sets determined with use of expression microarrays and ChIP-chip.

had previously been shown to exhibit Cbf1p-dependent chromatin remodeling (*20*). We predict that Cbf1 regulates a much smaller set of genes than ChIP-chip experiments do, but there is good agreement because more than 60% of the genes in our prediction were also found by ChIP-chip (Fig. 4F). We have thus shown that augmenting the consensus binding motifs with the new flanking bases revealed by the free energy landscapes results in concrete biological predictions that differentiate the function of Pho4 and Cbf1 and have broad agreement with the biological literature.

For two yeast TFs we have successfully predicted biological function by combining purely in vitro biophysical measurements with informatic knowledge of the organism's genome. As the theoretical and experimental tools of systems biology become more mature, this situation may become the rule rather than the exception, and it is worth considering whether there is any fundamental limit on the ability to predict biological behavior from in vitro measurements.

References and Notes

1. M. Kellis, N. Patterson, M. Endrizzi, B. Birren, E. S. Lander, *Nature* **423**, 241 (2003).
2. P. Cliften *et al.*, *Science* **301**, 71 (2003); published online 29 May 2003 (10.1126/science.1084337).
3. X. Xie *et al.*, *Nature* **434**, 338 (2005).
4. A. C. Gavin *et al.*, *Nature* **415**, 141 (2002).
5. Y. Ho *et al.*, *Nature* **415**, 180 (2002).
6. P. Uetz *et al.*, *Nature* **403**, 623 (2000).
7. C. T. Harbison *et al.*, *Nature* **431**, 99 (2004).
8. C. T. Workman *et al.*, *Science* **312**, 1054 (2006).
9. M. B. Elowitz, S. Leibler, *Nature* **403**, 335 (2000).
10. A. E. Mayo, Y. Setty, S. Shavit, A. Zaslaver, U. Alon, *PLoS Biol.* **4**, e45 (2006).
11. R. B. Jones, A. Gordus, J. A. Krall, G. MacBeath, *Nature* **439**, 168 (2006).
12. C. L. Warren *et al.*, *Proc. Natl. Acad. Sci. U.S.A.* **103**, 867 (2006).
13. S. Mukherjee *et al.*, *Nat. Genet.* **36**, 1331 (2004).
14. M. L. Bulyk, X. Huang, Y. Choo, G. M. Church, *Proc. Natl. Acad. Sci. U.S.A.* **98**, 7158 (2001).
15. C. Ponzetto *et al.*, *Cell* **77**, 261 (1994).
16. M. E. Massari, C. Murre, *Mol. Cell. Biol.* **20**, 429 (2000).
17. D. L. Levens, *Genes Dev.* **17**, 1071 (2003).
18. A. S. Carroll, A. C. Bishop, J. L. DeRisi, K. M. Shokat, E. K. O'Shea, *Proc. Natl. Acad. Sci. U.S.A.* **98**, 12578 (2001).
19. N. Ogawa, J. DeRisi, P. O. Brown, *Mol. Biol. Cell* **11**, 4309 (2000).
20. N. A. Kent, S. M. Eibert, J. Mellor, *J. Biol. Chem.* **279**, 27116 (2004).
21. M. Cai, R. W. Davis, *Cell* **61**, 437 (1990).
22. R. E. Baker, D. C. Masison, *Mol. Cell. Biol.* **10**, 2458 (1990).
23. D. S. Spinner, S. Liu, S. W. Wang, J. Schmidt, *J. Mol. Biol.* **317**, 431 (2002).
24. S. Park *et al.*, *Biochim. Biophys. Acta* **1670**, 217 (2004).
25. T. Thorsen, S. J. Maerkl, S. R. Quake, *Science* **298** 580 (2002); published online 26 September 2002 (10.1126/science.1076996).
26. Materials and methods are available on *Science* Online.
27. M. A. Unger, H. P. Chou, T. Thorsen, A. Scherer, S. R. Quake, *Science* **288**, 113 (2000).
28. M. Schena, D. Shalon, R. W. Davis, P. O. Brown, *Science* **270**, 467 (1995).
29. A. R. Ferre-D'Amare, G. C. Prendergast, E. B. Ziff, S. K. Burley, *Nature* **363**, 38 (1993).
30. T. Shimizu *et al.*, *EMBO J.* **16**, 4689 (1997).
31. M. L. Bulyk, P. L. Johnson, G. M. Church, *Nucleic Acids Res.* **30**, 1255 (2002).
32. T. K. Man, G. D. Stormo, *Nucleic Acids Res.* **29**, 2471 (2001).
33. P. V. Benos, M. L. Bulyk, G. D. Stormo, *Nucleic Acids Res.* **30**, 4442 (2002).
34. S. Sinha, M. Tompa, *Nucleic Acids Res.* **30**, 5549 (2002).
35. O. Elemento, S. Tavazoie, *Genome Biol.* **6**, R18 (2005).
36. J. A. Granek, N. D. Clarke, *Genome Biol.* **6**, R87 (2005).
37. M. Djordjevic, A. M. Sengupta, B. I. Shraiman, *Genome Res.* **13**, 2381 (2003).
38. We thank B. Wold and J. Berger for helpful discussions and K. Kapur and C. Jacobs for help with the document. Supported in part by Defense Advanced Research Projects Agency–Biological Input Output Systems, an NIH Director's Pioneer Award, and Howard Hughes Medical Institute. S.R.Q. holds equity in, is a paid consultant for, and is a co-founder and former director of Fluidigm, which may license the device described in this paper.